Annals of Biomedical Engineering, Vol. 44, No. 10, October 2016 (© 2016) pp. 2887–2900
DOI: 10.1007/s10439-016-1599-1

Hierarchical CT to Ultrasound Registration of the Lumbar Spine: A Comparison with Other Registration Methods

TERRY K. KOO[1] and WINGCHI EDMUND KWOK[2,3]

[1]Foot Levelers Biomechanics Research Laboratory, New York Chiropractic College, 2360 State Route 89, Seneca Falls, NY 13148, USA; [2]Department of Imaging Science, University of Rochester, Rochester, NY, USA; and [3]Rochester Center of Brain Imaging, University of Rochester, Rochester, NY, USA

(*Received 18 December 2015; accepted 24 March 2016; published online 28 March 2016*)

Associate Editor Karol Miller oversaw the review of this article.

Abstract—Three-dimensional (3D) measurement of the spine can provide important information for functional, developmental, diagnostic, and treatment-effect evaluations. However, existing measurement techniques are either 2-dimensional, highly invasive, or involve a high radiation dose, prohibiting their widespread and repeated use in both research and clinical settings. Non-invasive, non-ionizing, 3D measurement of the spine is still beyond the current state-of-the-art. Towards this goal, we developed an intensity-based hierarchical CT-ultrasound registration approach to quantify the 3D positions and orientations of lumbar vertebrae from 3D freehand ultrasound and one-time computed tomography. The method was validated using a human dry bone specimen (T12-L5) and a porcine cadaver (L2-L6) by comparing the registration results with a gold standard fiducial-based registration. Mean (SD) target registration error and percentage of successful registration were 1.2 (0.6) mm and 100% for the human dry bone specimen, and 2.18 (0.82) mm and 92% for the porcine cadaver, indicating that the method is accurate and robust under clinically realistic conditions. Given that the use of ultrasound eliminates ionizing radiation during pose measurements, we believe that the hierarchical CT-ultrasound registration method is an attractive option for quantifying 3D poses of individual vertebra and motion segment, and thus warrants further investigations.

Keywords—Image registration, Ultrasound, Computed tomography, Lumbar vertebra, Motion segment.

INTRODUCTION

The spine is a complex structure. It comprises a series of vertebrae, each with 6 degrees of freedom (DOF), which are linked by intervertebral discs, zygapophysial joints, ligaments, and muscles. Given its anatomical complexity, extensive degrees of freedom, and voluminous soft tissue content, precise pose measurements of the spine continue to be challenging. Nonetheless, such measurements can provide important information for image-guided navigation as well as functional, developmental, diagnostic, and treatment-effect evaluations. For instance, this information can be used to guide percutaneous spinal injection[26] and pedicle screw insertion.[10] It can also facilitate objective assessment of spinal deformities[3] (e.g., scoliosis) and aid in preoperative planning of deformity correction.[1] Such information may also be used to quantify spinal instability, which has been implicated as an important mechanical cause of back and neck pain.[7]

Current clinical practice relies primarily on coronal plane radiograph to quantify scoliotic deformities and sagittal plane flexion–extension radiograph to evaluate spinal instability. However, two-dimensional (2D) radiographs cannot detect out-of-plane deformities and coupled motions. It is well known that scoliotic curvature is not only a sideways deformity, but also involves rotation and displacement in other planes.[32] Biomechanical studies also revealed that a radial tear of the annulus fibrosis can markedly reduce resistance to axial rotation but flexion–extension is only marginally affected,[12] indicating that axial rotation is a more relevant measure of spinal instability.

To overcome the limitations of 2D radiographs, substantial research efforts have been made to measure the spine in a three-dimensional (3D) manner. However, existing methods such as bi-plane radiography, repetitive computed tomography (CT) imaging, and implanted marker tracking *etc.* are either highly inva-

Address correspondence to Terry K. Koo, Foot Levelers Biomechanics Research Laboratory, New York Chiropractic College, 2360 State Route 89, Seneca Falls, NY 13148, USA. Electronic mail: tkoo@nycc.edu

sive[5] or involve a high radiation dose,[11,13,18,21,23] prohibiting their widespread and repeated use in both research and clinical settings. Non-invasive, non-ionizing, 3D measurement of the spine is still beyond the current state-of-the-art.

Three-dimensional freehand ultrasound appears to be an attractive imaging method towards this goal. Briefly, 3D freehand ultrasound is a portable, non-invasive, and non-ionizing imaging technology that has recently been used to acquire 3D anatomical information of the patient during surgery. It can be achieved by equipping position sensors to a conventional 2D ultrasound system. Despite its advantages for patients and clinicians, it suffers from poor image quality. Hence, it is difficult to solely rely on 3D freehand ultrasound to precisely quantify the 3D poses of individual vertebra. To alleviate this problem, several CT-ultrasound registration approaches have been suggested. Much of the early work on CT-ultrasound registration of bony structures was based on feature-based registration.[19,31] This approach relies on extracting bone surfaces from both ultrasound and CT data, and registering them using iterative closest point algorithms. A major challenge of feature-based CT-ultrasound registration is the difficulty of accurately extracting bone surfaces from ultrasound images. More recently, intensity-based registration techniques have been developed to eliminate the need of segmenting bone surfaces from ultrasound data.[2,28,33,36] These techniques assume that the brightest pixels in ultrasound images are most often caused by the reflection of ultrasound waves on bone surfaces, and hence, extracted bone surfaces from CT images may be registered with an ultrasound dataset by maximizing the average intensity of the overlapping pixels. However, due to speckle noise and other artifacts, intensity of some regions within the overlying soft tissue can be brighter than bone surfaces in B-mode ultrasound, making the *in situ* application of pure intensity-based CT-ultrasound registration approach[2] problematic. In this study, we proposed an intensity-based hierarchical CT-ultrasound registration approach to overcome this technical challenge. Our objectives were: (1) To develop an intensity-based hierarchical CT-ultrasound registration method for 3D measurements of the lumbar spine; and (2) To evaluate its accuracy and robustness by comparing the results with ground truth solutions. We hypothesize that this new registration approach can be applied to the field of biomechanics to accurately quantify 3D poses of the lumbar spine.

MATERIALS AND METHODS

Overview

The basic premise of our approach to quantify 3D positions and orientations of individual vertebra is to match 3D freehand ultrasound images with a subject-specific geometrical model of the vertebra reconstructed from CT images. Given that only 3D freehand ultrasound is used during pose measurements, this approach allows for repeated measurements in a non-ionizing manner. Note also that CT scan is a one-time event in our approach. Hence, it is especially beneficial to those who have already taken a CT scan of their spine for other reasons. A flowchart illustrating the overview of our hierarchical CT-ultrasound registration method is shown in Fig. 1.

Details of the acquisition and processing of 3D ultrasound and CT volumetric images, as well as the hierarchical registration process are described below.

3D Ultrasound

A freehand 3D ultrasound system developed by our group[16] is used to acquire a 3D ultrasound dataset of the lumbar spine. The system consists of an ultrasound scanner (Ultramark 400c; ATL Ultrasound Inc., Bothell, WA) with a 3.5–5 MHz curvilinear transducer to image the lumbar spine, an optoelectronic measurement system (Northern Digital Inc., Waterloo, Canada) to track the transducer, and a personal computer with a frame grabber (PCI-1411) and a data acquisition card (PCI 6024E) (National Instruments Corporation, Austin, TX) installed to capture ultrasound images and synchronize with the tracking data. Transducer tracking is achieved via 5 non-coplanar infrared diodes (IRED) rigidly mounted on the transducer. A local coordinate system is embedded within the transducer so that its x and y axes align with the horizontal and vertical directions of the acquired ultrasound images respectively and its origin is at the center of the most convex point on the transducer's scanning surface. Local coordinates of each pixel from each ultrasound image are transformed to a common laboratory coordinate system using the tracking information, forming a 3D ultrasound dataset. The dataset is re-scaled to a pixel size of 0.5×0.5 mm and the resulting 3D ultrasound dataset is used in the final phase of the hierarchical registration to compute a final solution (Fig. 1, Phase 3).

The re-scaled 3D ultrasound dataset is also processed by a backward ray tracing method[35] to extract the pixels around the posterior vertebral surface.

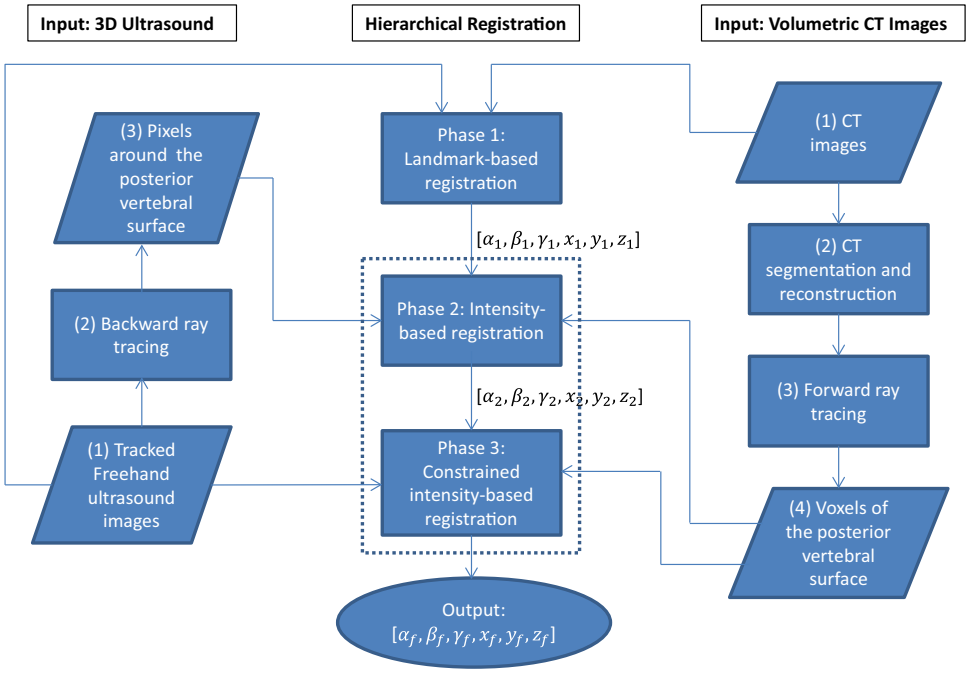

FIGURE 1. Workflow of the hierarchical CT to ultrasound registration algorithm. For each vertebra, the process begins with finding a reasonable initial guess of 3 translational and 3 rotational parameters that roughly transform each CT-reconstructed vertebra to the laboratory space of the actual assessment. This is accomplished by registering 3 corresponding bony landmarks between the ultrasound and CT dataset. We then refine the translational and rotational parameters by registering the voxels that represent the posterior surface of the CT-reconstructed vertebra to those extracted ultrasound pixels that roughly represent the vicinity of the posterior vertebral surface. Lastly, we apply a constrained intensity-based registration to the original ultrasound dataset to further refine the 3D positions and orientations of each vertebra by maximizing the average gray value of all ultrasound pixels that overlap with the posterior vertebral surfaces of the CT-based geometrical model. [α, β, γ] are the Euler angles in *Z-Y-X* sequence that specify the orientation of the anatomical coordinate system of the CT-reconstructed vertebral model with respect to the laboratory coordinate system. [*x*, *y*, *z*] are the vector that locates the origin of the anatomical coordinate system with respect to the laboratory coordinate system. Hence, [α, β, γ, *x*, *y*, *z*] are a set of transformation parameters that define the position and orientation of a target vertebra in the laboratory space. Subscripts 1 and 2 denote the intermediate solutions after the landmark-based and intensity-based registrations respectively, and subscript f represents the final solution after constrained intensity-based registration.

Briefly, the backward ray tracing method makes use of the distinct characteristics of bone in B-mode ultrasound (i.e., bright at the location of bone surface and dark directly underneath the bone surface) to help detect and extract the posterior vertebral surfaces. For each ultrasound image, a ray line is simulated along each pixel column to travel from the bottom to the top. As the ray line travels upwards, it is expected to transverse through a shallow region before reaching the bone surface. Hence, by selecting an intensity threshold which delineates the bone surfaces from the shallow region, we extract 10 pixels above and 10 pixels below the first pixel that exceed the intensity threshold (counting from bottom) to represent the vicinity of the posterior vertebral surface. This process is repeated for each pixel column of the image stack, and the extracted pixels are regarded as an extracted ultrasound dataset (Fig. 2). We evaluated 16 auto-thresholding methods[17] available in ImageJ (NIH, Bethesda, MD) and noted that "Percentile" and "Intermodes" methods work best for the porcine cadaver and human dry bone specimen respectively, and hence, they were used in our validation experiments (see "Experimental Validation" section). Details about these methods can be found elsewhere.[6,24]

Computed Tomography

Axial volumetric images of the vertebrae of interest with slice thickness of 1 mm and in-plane resolution of 0.5 × 0.5 mm are obtained from a Philips Brilliance 64-channel CT scanner (Philips Healthcare, Best, Netherlands). CT images are segmented semi-automatically by 3D Doctor software (Able software Corp., Lexington, MA) using a threshold-based interactive segmentation algorithm, and extracted boundaries of each vertebra are volume-rendered to create a solid model. We improved the forward ray tracing method proposed by Brendel *et al.*[2] to extract the posterior surface of each vertebra from the CT-reconstructed solid model. Briefly, we first rotate the CT-reconstructed solid model of each vertebra to match

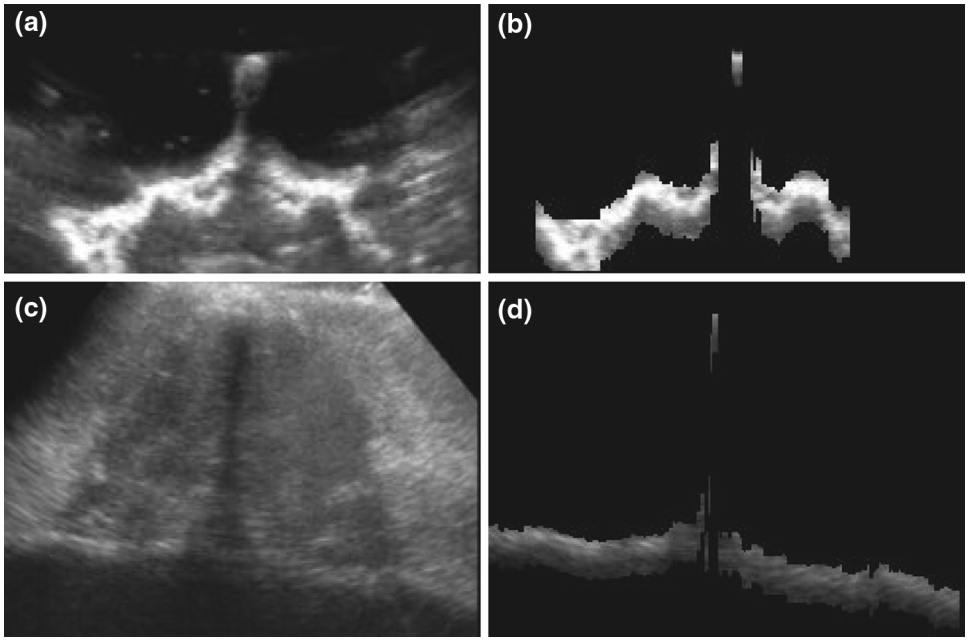

FIGURE 2. Sample ultrasound images from the original and extracted ultrasound dataset of the human dry bone and porcine cadaver. (a) Original and (b) extracted image of a human dry bone vertebra; (c) original and (d) extracted image of a porcine vertebra.

with the orientation observed in ultrasound images. Incidence of an ultrasound wave is then simulated on the solid model to extract the voxels that correspond to the unblocked posterior surface of each vertebra. To account for the reflection behavior of ultrasound, only those voxels that are within ±60° to the direction of incidence are retained.[2] Lastly, the extracted voxels are transformed back to their original coordinates for later registration use.

To facilitate the quantification of intervertebral poses, we define an anatomical coordinate system for each vertebra using the information from all voxels of the CT-reconstructed solid model. Origin of the anatomical coordinate system is defined as the centroid of the solid model. A set of three orthogonal axes representing the major axes of mass distribution within each vertebra (i.e., principal axes) are calculated using the principal axis transformation technique.[27,30] Assuming each voxel is a unit mass, the principal axes of a vertebra are the 3 eigenvectors of the following covariance matrix:

$$\begin{bmatrix} \sum x^2 & \sum xy & \sum xz \\ \sum xy & \sum y^2 & \sum yz \\ \sum xz & \sum yz & \sum z^2 \end{bmatrix} \tag{1}$$

where (x, y, z) represent the coordinates of each voxel of the target vertebra relative to its centroid. Summation within each element of the covariance matrix is performed over all segmented voxels. We define the x, y, and z axes of each vertebra as the calculated principal axes that point to the right, anterior, and superior directions respectively (Fig. 3).

Hierarchical CT to Ultrasound Registration

Landmark-Based Registration

The hierarchical CT to ultrasound registration algorithm starts with a landmark-based registration of 3 bony landmarks to get an initial estimate of 3 rotational and 3 translational parameters that transform the CT-based vertebral model to the laboratory space. This can be achieved by digitizing the coordinates of the spinous process (SP), the left transverse process (TP) and the right TP from both the CT and ultrasound dataset. A nonlinear optimization is then applied to search for a set of rotational (α, β, γ) and translational (x, y, z) parameters that minimize the average distance of the 3 pairs of bony landmarks ($\boldsymbol{D}_{\mathrm{a}}$) using the following objective function:

$$\begin{aligned} &\text{Minimizing} \quad \boldsymbol{D}_{\mathrm{a}}(\alpha, \beta, \gamma, x, y, z) \\ &= \frac{1}{3}\sum\nolimits_{i=1}^{3} \boldsymbol{D}\left(p_i^L, \boldsymbol{R}(\alpha, \beta, \gamma) \cdot p_i^v + \boldsymbol{T}(x, y, z)\right) \end{aligned} \tag{2}$$

where p_i^v (i stands for 1 = SP, 2 = left TP, 3 = right TP) is the coordinates of the bony landmark i (in anatomical coordinate system of the target vertebra)

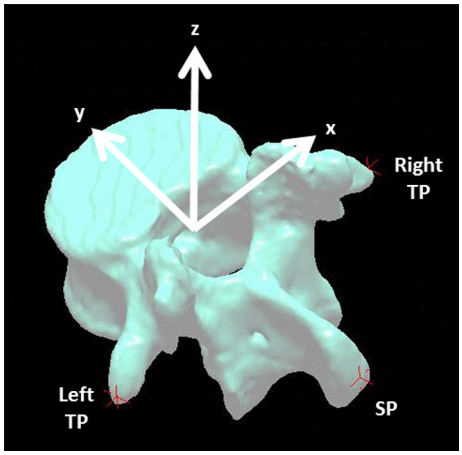

FIGURE 3. An anatomical coordinate system of a vertebra. The *x*, *y*, and *z* axes are defined as the calculated principal axes that point to the right, anterior, and superior directions respectively. Landmarks that were used for landmark-based registration are also shown.

digitized from the CT-based geometrical model, p_i^L is the coordinates of the same landmark i (in laboratory coordinate system) digitized from the ultrasound dataset; $\boldsymbol{R}$ is a 3 × 3 rotation matrix, which depends on *Z-Y-X* Euler angles α, β, and γ; $\boldsymbol{T}$ is a translation vector = $[x,\ y,\ z]'$, which locates the origin of the anatomical coordinate system with respect to the laboratory coordinate system, and $\boldsymbol{D}$ stands for the distance between the same landmarks after the transformation is applied to p_i^y.

Solution of the landmark-based registration $[\alpha_1, \beta_1, \gamma_1, x_1, y_1, z_1]$ is then used as an initial guess of the next phase of the hierarchical registration.

Stepwise Intensity-Based Registration

The stepwise intensity-based registration starts with the approach proposed by Yan *et al.*[36] to guide the search of a set of translational and rotational parameters $[\alpha_2, \beta_2, \gamma_2, x_2, y_2, z_2]$ closest to the ground truth. This is achieved by applying the backward ray tracing method described in "3D Ultrasound" section to extract the ultrasound pixels in the vicinity of the posterior vertebral surface and use them to register with the posterior vertebral surface extracted from the CT volume. Next we constrain our search space within ±8°/8 mm at each degree-of-freedom (DOF) (i.e., $\alpha_2 \pm 8°$, $\beta_2 \pm 8°$, $\gamma_2 \pm 8°$, $x_2 \pm 8$ mm, $y_2 = \pm 8$ mm, $z_2 \pm 8$ mm) and re-register the extracted posterior surfaces of the CT-based model with the original ultrasound dataset to get the final solution $[\alpha_f, \beta_f, \gamma_f, x_f, y_f, z_f]$.

Objective function for both phases of the stepwise intensity-based registration can be written as:

$$\text{Maximizing} \quad \boldsymbol{I}(\alpha, \beta, \gamma, x, y, z) = \frac{1}{N}\sum_{i=1}^{N} \boldsymbol{F}(\boldsymbol{R}(\alpha, \beta, \gamma) \cdot \bar{p}_l + \boldsymbol{T}(x, y, z)) \tag{3}$$

Herein, $\bar{p}_l$ (for $i = 1$ to N) represents the coordinates of all voxels of the CT-based model that correspond to the extracted posterior surfaces of a target vertebra. Their coordinates are expressed in terms of the anatomical coordinate system of the target vertebra. R is a rotation matrix, which depends on Euler angles α, β, and γ. $\boldsymbol{T}$ is a translation vector = $[x, y, z]'$, which locates the origin of the anatomical coordinate system with respect to the laboratory coordinate system. F(p) is a function that determines the value of the closest point to p within the ultrasound dataset using the nearest-neighbor algorithm. If the distance of the closest point from point p is less than 0.866 mm (i.e., the largest distance that a closest point is still within a 0.5 × 0.5 × 0.5 mm voxel), F(p) delivers the gray value of the closest point, otherwise, the gray value is set to zero. Note that the extracted and original ultrasound dataset are used in the 1st and 2nd phase of the stepwise intensity-based registration respectively. I represents the average gray value of the closest pixels.

For both intensity-based registration phases, the Nelder-Mead simplex method[20] is used to optimize the 3 rotational and 3 translational parameters. This optimization strategy has been widely used to find the minimum or maximum of a non-smooth objective function in multidimensional space, mainly because it does not require any calculation of function gradients.[29] The method has also been shown to perform well when the number of parameters to be optimized is relatively small (i.e., up to around 6 parameters).[22]

Experimental Validation

Accuracy and robustness of the hierarchical CT to ultrasound registration algorithm presented above was evaluated using a human dry bone specimen and a fresh porcine cadaver. Porcine spine was chosen as it is anatomically and functionally similar to the human spine and is frequently used as a substitute in experiments involving spine fusion and instrumentation technique.[4,35]

Human Dry Bone Specimen

A human dry bone specimen (T12-L5) (The Bone Room, Berkeley, CA) was positioned to overlap at their facet joints and secured inside a plastic box to mimic a realistic *in situ* scenario (Fig. 4). Axial volumetric CT images of the dry bone specimen were acquired and voxels of the posterior surface of each

vertebra were extracted as described in "Computed Tomography" section. Six ultrasound scans of the specimen were then acquired by the freehand 3D ultrasound system. During each ultrasound scan, the specimen was submerged in water, and axial ultrasound images were acquired for 30 s at a frame rate of 30 Hz (i.e., 900 images in total) with the transducer positioned posterior to spinous processes and slowly swiped along the specimen from L5 to T12. Separate registration was performed on each vertebra. To speed up the registration process, only a subset of ultrasound images that covered the vertebra to be registered was included for each registration. Selection of the image subset was achieved by visually inspecting the 3D ultrasound dataset. Given that intensity-based registration relies on maximizing the average intensity of all ultrasound pixels that overlap with the extracted posterior surface from the CT-reconstructed vertebral model, overlaps of articular processes at zygapophysial joints would have minimal effects to the registration. Hence, the image selection does not have to be precise.

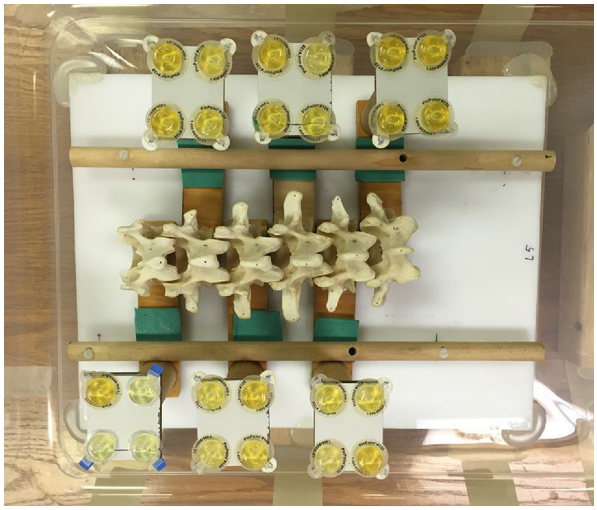

FIGURE 4. Experimental setup of the human dry bone experiment.

To quantify the accuracy of the hierarchical CT to ultrasound registration algorithm, 4 fiducial markers (Pinpoint® 128, Beekley Medical, Bristol, CT) were rigidly attached to each vertebra to enable the computation of a ground truth. This was achieved by gluing the vertebra to one end of a wood plate and securing the fiducial markers to the other end (Fig. 4). The unique conical design of the Pinpoint® 128 allowed for precise localization of the fiducial coordinates in CT images. Its central hole also facilitated accurate digitization of the fiducial coordinates in the laboratory space during the ultrasound experiment. The corresponding fiducial coordinates were paired up to compute the rotational and translational parameters that minimized the average distance among fiducial pairs. The fiducial-based registration solution is regarded as the ground truth.[35,36]

Porcine Cadaver

In addition to the dry bone experiment, we took our validation a step further to evaluate the *in situ* performance of our hierarchical CT-ultrasound registration algorithm using a lumbosacral section of a fresh porcine cadaver obtained from a local abattoir. To enable the computation of the ground truth solution, we rigidly mounted 4 fiducial markers to each vertebra by (1) exposing the anterior surface of each lumbar vertebral body; (2) anchoring a plastic post (made from pipette tip) into each lumbar vertebral body; and (3) press-fitting a fiducial marker post to each plastic post on L2-L6.

A CT scan was acquired with the specimen placed in a supine position inside a plastic box (Fig. 5a) using the settings described in "Computed Tomography" section. During the ultrasound experiment, the specimen was stabilized in a prone position with the spinous processes faced up, the sacral end supported by a side table, and a plastic post of L1 hanging on a side bar (Fig. 5b). Axial ultrasound images were then acquired for 30 s at a frame rate of 30 Hz with the transducer slowly swiped along the specimen from L2 to L6. Scans were repeated 5 times. Fiducial marker coordinates

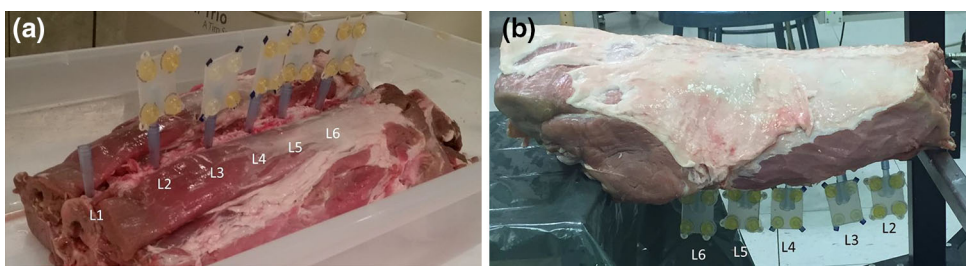

FIGURE 5. Experimental setup of the porcine cadaver experiment. (a) During CT scan, the lumbosacral section was placed in a supine position. (b) During ultrasound scan, the cadaver was placed in a prone position.

were digitized before and after the ultrasound scans and their average was used to compute the ground truth.

Quantitative Analysis

Performance of the hierarchical registration method was compared with those of a landmark-based registration, a pure intensity-based registration (i.e., Brendal *et al.*[2]) and a modified intensity-based registration approach (i.e., Yan *et al.*[36]).

We defined target registration error (TRE) as root mean square of the distances between coordinates of all voxels of the CT-reconstructed solid model transformed by the fiducial registration (i.e., ground true) and our registration transformations, and used TRE as a quantitative measure of the overall performance of each registration method. For both the human dry bone and porcine cadaver experiments, one-way repeated measures ANOVA ($\alpha = 0.05$) were performed to test the effect of registration approach on TRE. Post-hoc comparisons were based on paired t tests with Bonferroni correction. In addition, we regarded TRE less than 3 mm as successful registration,[25] and compared the percentage of successful registration among different registration approaches.

Accuracy of each registration method at each DOF (i.e., Euler angles α, β, γ and translations x, y, z that define the orientation and position of a vertebra in the laboratory space) was determined by calculating the bias and repeatability, using the definitions of ISO 5725.[14,15] Bias at each vertebral level was defined as the difference between the average of n repeated measurements and the ground true (i.e., the fiducial-based registration solution). Given that bias can either be positive or negative, they were reported at each vertebral level to avoid cancellation effect.[15] Repeatability at each vertebral level was defined as the standard deviation of n repeated measurements. As suggested by ISO 5725-2, we reported the average repeatability value among all vertebral levels because repeatability is always a positive number.[14] Note that there were 6 and 5 repeated measurements per vertebra respectively for the human dry bone specimen ($n = 6$) and porcine cadaver ($n = 5$).

Motion segment poses were also determined by calculating the anatomical joint angles and intervertebral translations between each pair of adjacent vertebrae. Intervertebral translations (i.e., medial–lateral (ML), anterior-posterior (AP), and superior-inferior (SI) translations) were defined as the x, y, z components of the origin of the anatomical coordinate system of the superior vertebra with respect to the anatomical coordinate system of the inferior vertebra (e.g., L4 relative to L5). The method proposed by Grood and Suntay[9] was adopted to calculate the anatomical joint angles of each motion segment. Herein, flexion/extension and axial rotation are defined to take place about the x axis of the inferior vertebra and the z axis of the superior vertebra respectively, and lateral bending is the rotation about a floating axis that is perpendicular to both the flexion/extension and axial rotation axes. Again, accuracy of each registration method at each motion segment's DOF was determined by calculating the bias and repeatability, using the definitions in ISO 5725.

Qualitative Analysis

Given that there will be no ground truth to compare if the hierarchical registration method is applied to live subject, it is imperative to come up with a mean to check whether a registration solution makes sense. We developed a visualization tool to address this important requirement. The tool superimposes registered CT voxels of the posterior vertebral surface to the 3D ultrasound dataset as dark pixels (i.e., zero intensity), displays them as an image sequence, and hence, provides qualitative information for the evaluation of the validity of registration solutions.

RESULTS

Overall Performance

Sample registered images of a human vertebra (L5) as well as a porcine vertebra (L6) are shown in Fig. 6 to qualitatively illustrate the validity of the hierarchical CT to ultrasound registration solutions. Entire registered image sequences (Videos 1 and 2) are also included as supplementary materials. As revealed in Fig. 6, the superimposed CT voxels of the posterior vertebral surface match well with the ultrasound images of the corresponding posterior vertebral surface, indicating that the registration solutions are reasonable.

Figures 7 and 8 show the TRE of different registration approaches when they are applied to the human dry bone specimen and the porcine cadaver respectively. For the human dry bone specimen, registered vertebrae have a mean TRE (SD) of 5.57 (2.85) mm, 1.60 (1.15) mm, 1.05 (0.60) mm, and 1.12 (0.61) mm for the landmark-based, Yan, Brendel, and hierarchical registration approaches respectively. One-way repeated measures ANOVA reveals a significant difference among the registration approaches ($p < 0.001$). Post-hoc comparisons shows that TRE of the landmark-based registration is significantly larger than the other registration approaches ($p < 0.001$ for all paired comparisons), and the Brendel approach is signifi-

cantly better than Yan ($p = 0.012$), but it is not significantly different from the hierarchical registration approach ($p = 0.367$). In addition, the successful rate (i.e., TRE < 3 mm) of the landmark-based, Yan, Brendel, and hierarchical registration approaches are 11, 86, 100, and 100% respectively (Table 1). Taken together, it appears that all approaches, except for the landmark-based registration, are capable to provide accurate registration when applied to the human dry bone specimen, but the hierarchical registration and Brendel approaches appear to be the best.

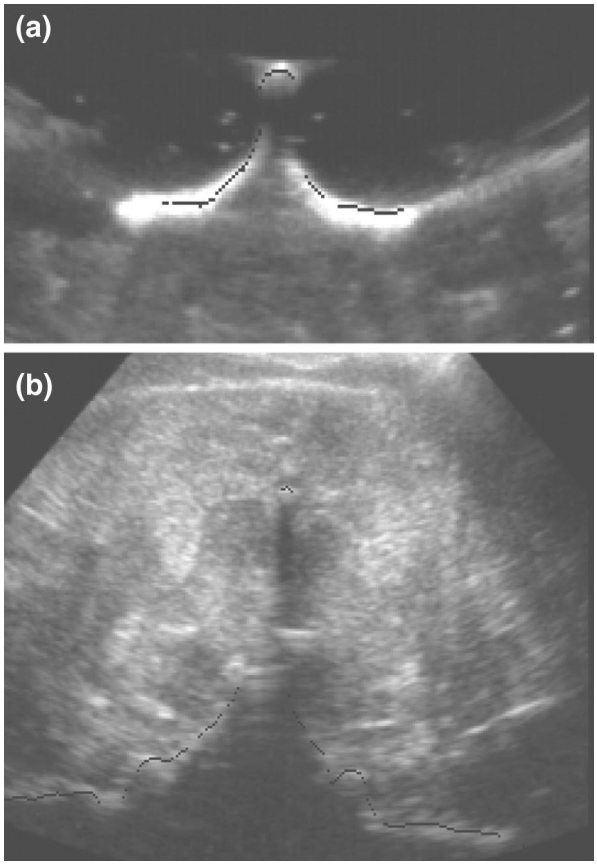

FIGURE 6. Sample registered ultrasound images of (a) human dry bone L5 vertebra and (b) porcine L6 vertebra. Note that registered CT voxels of the posterior vertebral surface are superimposed to the 3D ultrasound dataset as dark pixels (i.e., zero intensity). Entire registered image sequences (Videos 1 and 2) are also included as supplementary materials.

On the other hand, registered vertebrae of the porcine cadaver have a mean TRE (SD) of 6.26 (3.24) mm, 3.19 (1.08) mm, 24.96 (23.14) mm, and 2.18 (0.82) mm for the landmark-based, Yan, Brendel, and hierarchical registration approaches respectively, which are again statistically significantly different ($p < 0.001$). However, post hoc paired comparisons further reveal that the hierarchical registration outperforms the other approaches, the Yan approach ranks the second, followed by the landmark-based registration, and the Brendel approach is the worst ($p < 0.001$ in all paired comparisons). As expected, TRE of the porcine cadaver is always larger than that of the human dry bone specimen, no matter which registration approach is used. The successful rate of the hierarchical, Yan, landmark-based, and Brendel registration approaches are 92, 40, 32, and 8% respectively (Table 1), indicating that only the hierarchical registration approach can provide accurate and robust registration in real situations (i.e., vertebrae covered by soft tissues).

Performance at Each Degree-of Freedom

Bias

Figure 9 plots the biases of different registration approaches at each DOF (i.e., $\alpha, \beta, \gamma, x, y, z$) of each human dry bone vertebra. A similar plot of the porcine cadaver is shown in Fig. 10 to facilitate comparison. As revealed in Fig. 9, all approaches, except for the landmark-based registration, appear to perform very well at each DOF of each human dry bone vertebra. Specifically, biases of the hierarchical registration on the human dry bone specimen range between $-0.01°$ and $0.52°$ for Euler angle α, $-0.15°$ and $1.18°$ for Euler angle β, $-0.9°$ and $0.24°$ for Euler angle γ, -0.7 and 0.15 mm for x translation, -0.55 and 0.09 mm for y translation, and -1.36 and 0.16 mm for z translation respectively. However, Fig. 10 reveals that only the hierarchical registration performs well at each DOF of each porcine vertebra. Specifically, biases of the hierarchical registration on the porcine cadaver range between $-2.21°$ and $0.43°$ for α, $-0.81°$ and $1.69°$ for β, $-3.37°$ and $1.48°$ for γ, -1.32 and -0.03 mm for x, -0.66 and 1.37 mm for y, and -1.12 and -0.26 mm

TABLE 1. Comparison of registration performance between landmark-based, Yan, Brendel, and hierarchical registration methods. A registration with TRE < 3 mm is regarded as successful.

	Human dry bone specimen		Porcine cadaver	
Registration Method	TRE Range (mm)	Successful rate (%)	TRE Range (mm)	Successful rate (%)
Landmark-based	2.57–13.58	11	1.81–11.66	8
Yan	0.33–5.10	86	1.06–5.39	40
Hierarchical	0.37–2.90	100	0.89–4.45	92
Brendel	0.22–2.68	100	1.48–57.58	32

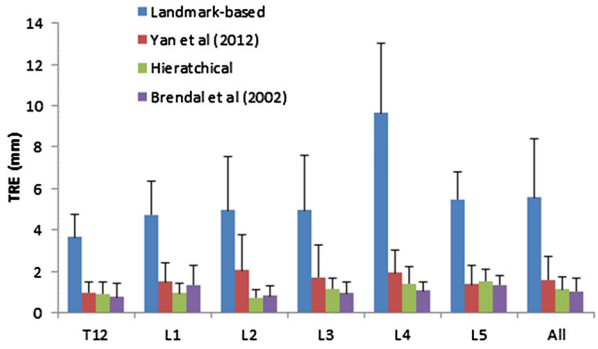

FIGURE 7. Mean and standard deviation of the target registration error (TRE) of the human dry bone specimen.

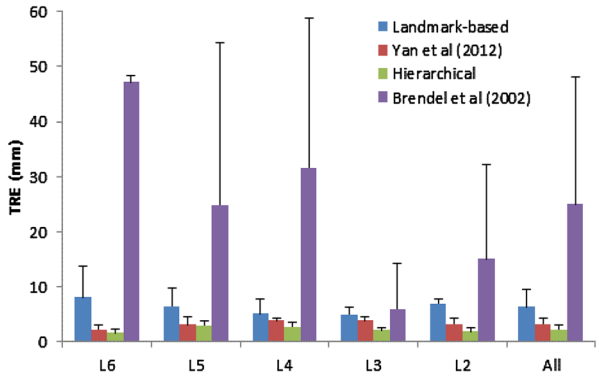

FIGURE 8. Mean and standard deviation of the target registration error (TRE) of the porcine cadaver.

for z respectively. The Brendel approach performs poorly in terms of bias, which is even inferior to the landmark-based registration. Biases of the Yan approach appear to be small at all DOFs except for γ, which ranges between $-7.32°$ and $4.15°$ among the tested vertebrae.

In terms of motion segment measurements, Fig. 11 reveals that biases of all except for the landmark-based registration approach appear to be small at each DOF of each motion segment of the human dry bone specimen. However, only the hierarchical registration performs satisfactory at each DOF of each motion segment of the porcine cadaver (Fig. 12). Specifically, biases of the hierarchical registration range between $-0.46°$ and $0.95°$ for flexion/extension, $-1.29°$ and $1.01°$ for lateral bending, $-0.42°$ and $0.32°$ for axial rotation, -1.45 and 0.40 mm for ML translation, -0.45 and 0.70 mm for AP translation, and -0.56 and -0.08 mm for SI translation respectively for the human dry bone specimen, and between $-3.85°$ and $2.56°$ for flexion/extension, $-2.47°$ and $2.27°$ for lateral bending, $-2.61°$ and $1.79°$ for axial rotation, -1.66 and 0.68 mm for ML translation, -2.14 and 0.60 mm for AP translation, and -0.91 and 1.94 mm respectively for the porcine cadaver.

Repeatability

Table 2 compares the repeatability of different registration approaches for the quantification of vertebral positions and orientations. For the human dry bone specimen, it appears that the repeatability of both Brendel and hierarchical registration approaches are excellent at each DOF. For instance, repeatability of the hierarchical registration for $\alpha, \beta, \gamma, x, y, z$ on human dry bone specimen are $0.32°$, $0.74°$, $1.16°$, 0.26, 0.4, and 0.66 mm respectively. For the porcine cadaver, the hierarchical registration is again considered to be highly repeatable with values of $0.95°$, $1.29°$, $0.94°$, 0.62, 0.59, and 1.20 mm respectively for $\alpha, \beta, \gamma, x, y$, and z. However, the Brendel approach performs poorly on the porcine cadaver, which is even poorer than the landmark-based approach.

In terms of motion segment measurements, the repeatability of the hierarchical registration approach for both the human dry bone specimen and the porcine cadaver appears to be the best among all tested registration methods (Table 3). Specifically, repeatability of the hierarchical registration for flexion/extension, lateral bending, axial rotation, ML translation, AP translation, and SI translation are $1.64°$, $1.26°$, $0.47°$, 0.53, 1.04, and 0.70 mm respectively for the human dry bone specimen, and $1.16°$, $1.58°$, $1.76°$, 1.57, 1.20, and 1.52 mm respectively for the porcine cadaver. For the Brendel approach, motion segment pose measurements are only repeatable on the human dry bone specimen, but not on the porcine cadaver.

Run Time

In this study, we used a Windows based laptop computer with an Intel Core i5-4310U (2.6 GHz) to run all registrations. The run time is primarily dependent on the size of the ultrasound dataset to be registered. On average, each phase of the stepwise intensity-based registration takes about 50 s to complete, leading to the total registration time of 100 s per human vertebra. This run time indicates that the hierarchical CT-ultrasound registration is time-efficient, which is beneficial for clinical applications.

DISCUSSION

In this study, we have successfully developed a hierarchical CT to ultrasound registration approach to accurately quantify the 3D positions and orientations of the lumbar spine. The method was validated using

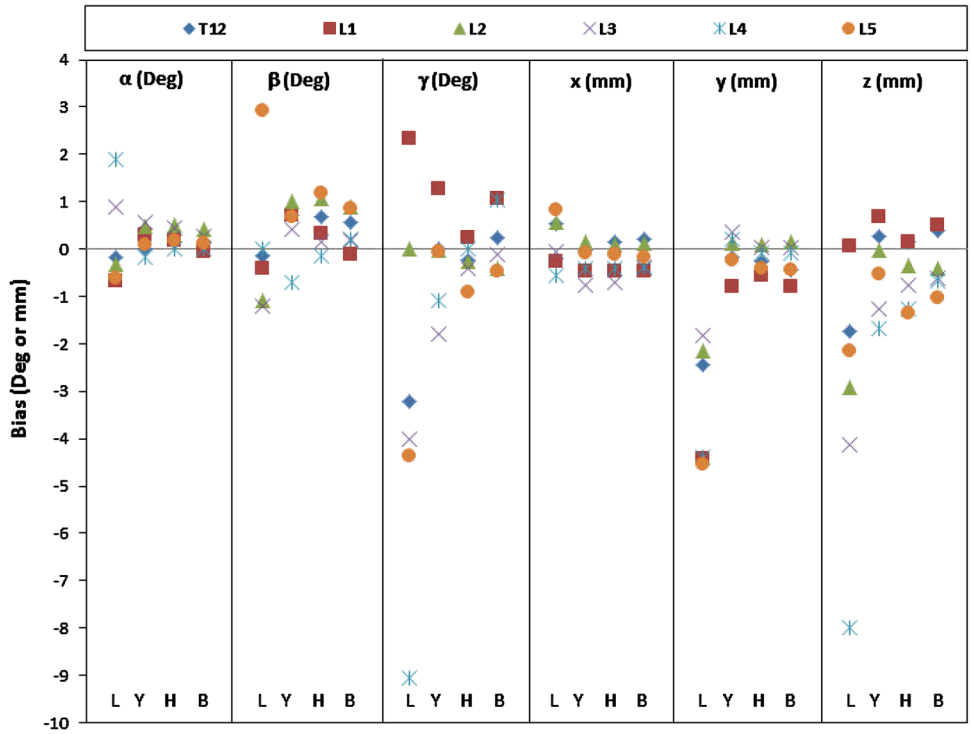

FIGURE 9. Biases of different registration approaches for the quantification of 3D positions and orientations of the human dry bone vertebrae. Biases at each degree of freedom (α, β, γ, *x*, *y*, *z*) are grouped from left to right. For each degree of freedom, from left to right, biases of each registration method (*L* Landmark-based, *Y* Yan, *H* Hierarchical, and *B* Brendel) on each vertebra (T12, L1, L2, L3, L4, L5) are plotted.

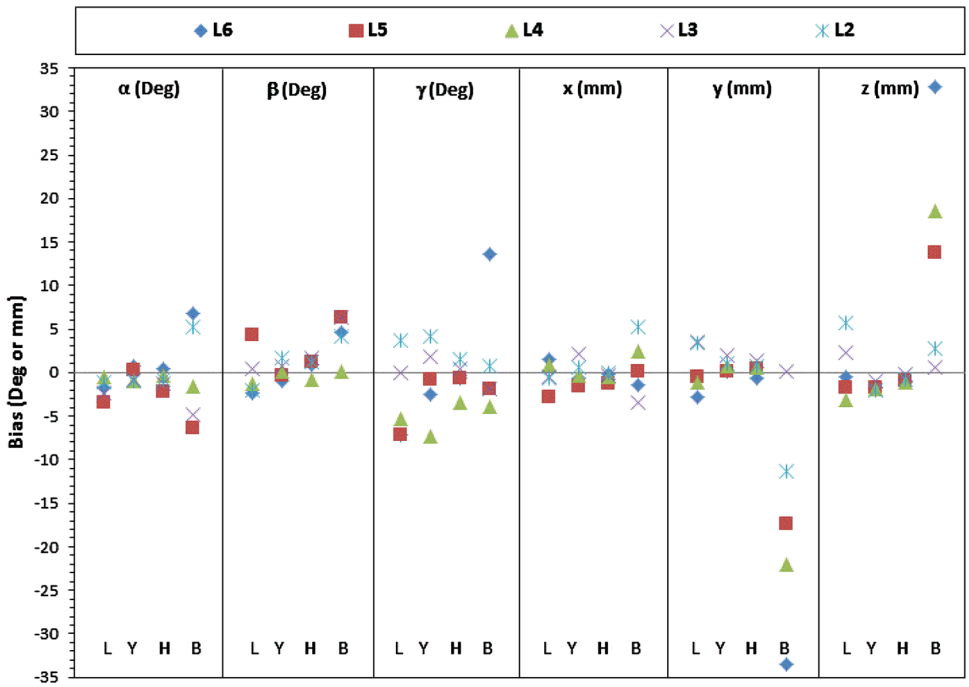

FIGURE 10. Biases of different registration approaches for the quantification of 3D positions and orientations of porcine vertebrae. Biases at each degree of freedom (α, β, γ, *x*, *y*, *z*) are grouped from left to right. For each degree of freedom, from left to right, biases of each registration method (*L* Landmark-based, *Y* Yan, *H* Hierarchical, and *B* Brendel) on each vertebra (L2, L3, L4, L5, L6) are plotted.

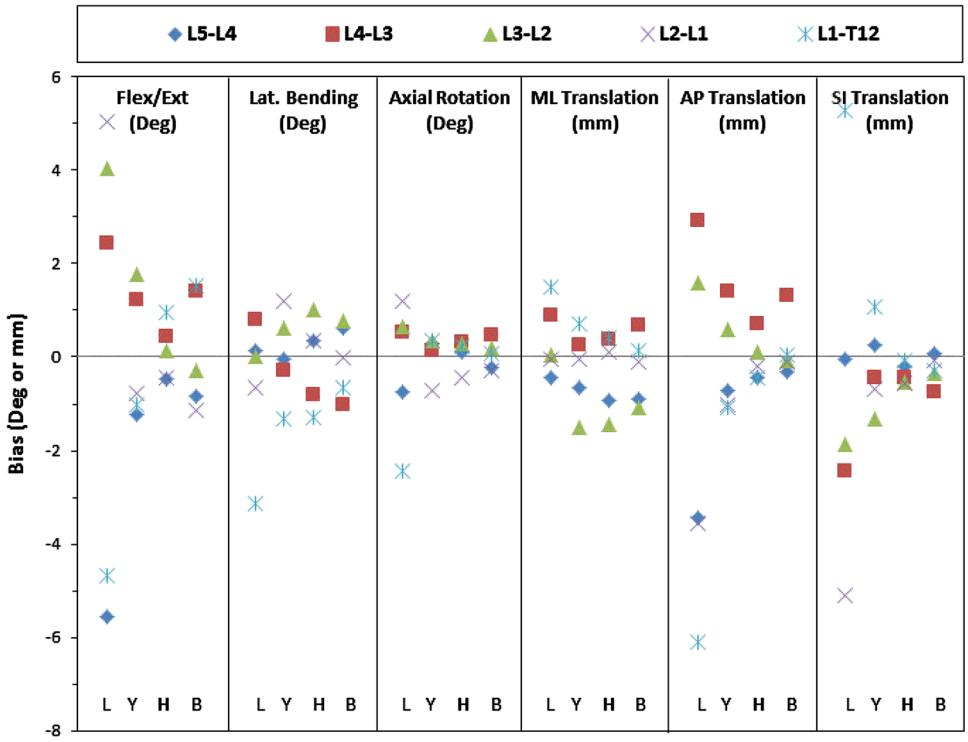

FIGURE 11. Biases of different registration approaches for the quantification of motion segment poses of the human dry bone specimen. Biases at each degree of freedom (flexion/extension, lateral bending, axial rotation, anterior-posterior translation, medial–lateral translation, superior-inferior translation) are grouped from left to right. For each degree of freedom, from left to right, biases of each registration method (*L* Landmark-based, *Y* Yan, *H* Hierarchical, and *B* Brendel) on each motion segment (L5-L4, L4-L3, L3-L2, L2-L1, L1-T12) are plotted.

both dry bone specimen and porcine cadaver, and compared with 3 registration methods reported in the literature. Unlike other validation studies[8,25,35,36] which randomly generated initial misalignments within certain limit from the ground truth to evaluate the accuracy and robustness of their registration CT-ultrasound approaches, we opted to determine an initial guess using the actual measurement protocol (i.e., landmark-based registration) so that the real performance of the hierarchical registration method can be better evaluated. Results of our validation experiments demonstrated that the hierarchical CT-ultrasound registration is the only method that is accurate and robust under both experimental conditions. Given that these registration methods are ultimately aimed to apply to live human subjects, our results highlight the importance of validating new registration techniques using a model that better mimics the real situation. For instance, if we only conducted the dry bone specimen experiment, we might have mistakenly concluded that the Brendel method is accurate and robust when applied to live human subjects.

The reason why the Brendel method does not work satisfactorily in the porcine cadaver is likely related to the speckle noises and artifacts of ultrasound images within soft tissues, making the gray values in some regions of soft tissues even brighter than the posterior bone surfaces, and hence, an intensity-based registration may converge toward these hyperechoic regions. Winter *et al.*[33] proposed to use adaptive depth gain compensation to enhance the bone surface in ultrasound images. However, their method requires subjective selection of tuning parameters and it is not known whether it would work satisfactorily if speckle noise and artifact are severe.[34] We overcome this problem by only extracting those pixels in the vicinity of the posterior surfaces of a vertebra and assigning the gray value of the rest of ultrasound pixels to zero. It is worth mentioning that the extracted pixels are by no means an accurate representation of the posterior vertebral surface. Nonetheless, our results demonstrate that they are adequate to facilitate the computation of an intermediate solution $[\alpha_2, \beta_2, \gamma_2, x_2, y_2, z_2]$ closest to the ground truth. We have also demonstrated that subsequent use of a constrained intensity-based registration to the original ultrasound dataset further improves the accuracy and robustness.

In this study, we restricted our search space in the final phase of the hierarchical registration within $\pm 8°$/8 mm of $[\alpha_2, \beta_2, \gamma_2, x_2, y_2, z_2]$. This selection was based on the fact that the differences between

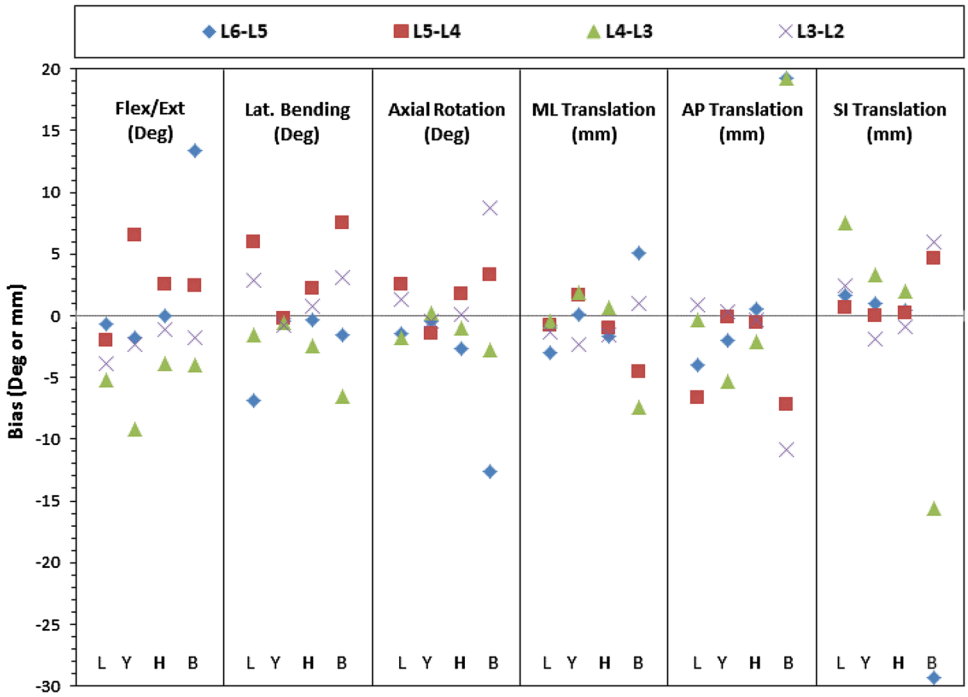

FIGURE 12. Biases of different registration approaches for the quantification of motion segment poses of the porcine cadaver. Biases at each degree of freedom (i.e., flexion/extension, lateral bending, axial rotation, anterior-posterior translation, medial–lateral translation, superior-inferior translation) are grouped from left to right. For each degree of freedom, from left to right, biases of each registration method (*L* Landmark-based, *Y* Yan, *H* Hierarchical, and *B* Brendel) on each motion segment (L6-L5, L5-L4, L4-L3, L3-L2) are plotted.

TABLE 2. Repeatability of different registration approaches for the quantification of vertebral positions and orientations

	α (°)		β (°)		γ (°)		x (mm)		y (mm)		z (mm)	
Registration method	H*	P#	H	P	H	P	H	P	H	P	H	P
Landmark-based	0.93	2.81	2.05	2.53	5.05	3.17	0.82	3.00	1.12	2.07	2.86	2.22
Yan	0.53	1.03	0.86	1.24	2.80	1.89	0.43	0.89	0.75	0.81	1.37	1.15
Brendel	0.36	5.71	0.85	6.19	1.20	6.46	0.30	5.53	0.43	13.07	0.70	9.52
Hierarchical	0.32	0.95	0.74	1.29	1.16	0.94	0.26	0.62	0.40	0.59	0.66	1.20

* H stands for human dry bone specimen; # P stands for porcine cadaver.

TABLE 3. Repeatability of different registration approaches for the quantification of motion segment poses

	Flex/Ext (°)		Lateral bending (°)		Axial rotation (°)		ML translation (mm)		AP translation (mm)		SI translation (mm)	
Registration method	H*	P#	H	P	H	P	H	P	H	P	H	P
Landmark-based	5.62	1.69	2.61	3.07	1.36	4.35	1.44	5.48	3.49	3.44	2.92	3.68
Yan	3.75	2.29	1.47	1.64	0.78	1.63	0.87	2.18	2.25	1.91	1.52	1.46
Brendel	2.09	10.22	1.45	12.28	0.49	7.23	0.58	10.19	1.16	18.72	0.80	16.48
Hierarchical	1.64	1.16	1.26	1.58	0.47	1.76	0.53	1.57	1.04	1.20	0.70	1.52

* H stands for human dry bone specimen; # P stands for porcine cadaver.

$[\alpha_2, \beta_2, \gamma_2, x_2, y_2, z_2]$ and the ground true solution at each DOF were well within $\pm 8°/8$ mm. Hence, our selection ensured that the search space covered the true solution yet minimized the chance of soft tissue noises and artifacts to mistakenly direct the optimization to an unrealistic solution.

Theoretically, an important factor that could affect the accuracy and robustness of the hierarchical CT-ultrasound registration method is whether there are any severe artifacts on or nearby the posterior surfaces of the vertebrae. For instance, inflammation and edema are likely to alter echoic responses of the affected tissues in B-mode ultrasound. Depending on the intensities and locations of these tissue alterations, they may or may not affect registration accuracy and robustness. However, given that metallic implants such as screws and plates are usually very bright in both CT and ultrasound, if they are in a closed proximity to the posterior vertebral surface, they are likely to affect registration accuracy and robustness. Nonetheless, separate studies are needed to fully evaluate the effects of tissue alterations and metallic implants on the registration accuracy and robustness of the hierarchical CT-ultrasound registration approach.

It is quite obvious that successful application of any CT-ultrasound registration method depends heavily on the quality of the acquired ultrasound data.[34] That would explain why both bias and repeatability of our hierarchical CT-ultrasound registration approach were consistently better on the human dry bone specimen. In ultrasound imaging, a major factor that limits the spatial resolution and visualization of details is the volume of the acoustic pulse. While axial resolution depends mainly on ultrasound frequency, lateral and elevational resolutions are depth dependent. Especially in the far field beyond the focal zone, the ultrasound beam diverges and substantially reduces both lateral and evolutional resolutions. It is worth to point out that porcine vertebrae are physically situated at much deeper locations than *in situ* human vertebrae. Therefore, we expect the bias and repeatability of the hierarchical CT-ultrasound registration on live human subjects to be between those of the human dry bone specimen and porcine cadaver reported in this study.

As expected, due to the potential cumulative effect of registration errors between adjacent vertebrae, both bias and repeatability of the hierarchical CT-ultrasound registration at the motion segment level appear to be inferior to those at the vertebral level. Nonetheless, repeatability of the hierarchical CT-ultrasound registration at each motion segment's DOF of the porcine cadaver was still pretty good (1.57 mm for ML translation, 1.20 mm for AP translation, 1.52 mm for SI translation, 1.16° for flexion–extension, 1.58° for lateral bending, and 1.76° for axial rotation) (Table 3). In addition, even in the worst case scenario, bias at each motion segment's DOF of the porcine cadaver was no more than 1.66 mm for ML translation, 2.14 mm for AP translation, 1.94 mm for SI translation, 3.85° for flexion–extension, 2.47° for lateral bending, and 2.61° for axial rotation (Fig. 10). These results indicate the potential of using the hierarchical CT-ultrasound registration approach to quantify 3D intersegmental poses.

To the author's knowledge, this is the first study that explicitly reports bias and repeatability of different CT-ultrasound registration approaches at each DOF of a vertebra as well as at each DOF of a motion segment. In terms of bias, repeatability, and robustness, our results clearly demonstrate that the hierarchical CT-ultrasound registration approach developed in this study is superior to the other tested CT-ultrasound registration methods under clinically realistic conditions. Given that the use of ultrasound eliminates ionizing radiation during pose measurements, we conclude that the hierarchical CT-ultrasound registration method is an attractive option for quantifying 3D poses of individual vertebra and motion segment, and thus warrants further investigations.

ELECTRONIC SUPPLEMENTARY MATERIAL

The online version of this article (doi: 10.1007/s10439-016-1599-1) contains supplementary material, which is available to authorized users.

ACKNOWLEDGMENTS

The authors would like to thank Dr. Jingyi Gao for her initial contribution of this work, Christopher Kirby, Weiling Zhang, Komal Khattak, and Nicholas Darcangelo for their assistance in data collection and analysis, Dr. Tom Foster, Erik Saluste, Angela Holland and Sandy Smashe for their involvements in arranging and performing the CT scans at Strong Memorial Hospital, and Anne Smith for her help on proofreading the manuscript. This work was supported by an intramural fund of New York Chiropractic College.

REFERENCES

[1]Aurouer, N., I. Obeid, O. Gille, V. Pointillart, and J. M. Vital. Computerized preoperative planning for correction of sagittal deformity of the spine. *Surg. Radiol. Anat.* 31:781–792, 2009.

[2]Brendel, B., S. Winter, A. Rick, M. Stockheim, and H. Ermert. Registration of 3D CT and ultrasound datasets of the spine using bone structures. *Comput. Aided Surg.* 7:146–155, 2002.

[3]Cobb, J. R. Outline for the study of scoliosis. *Instr. Course Lect.* 5:261–275, 1948.

[4]Dath, R., A. D. Ebinesan, K. M. Porter, and A. W. Miles. Anatomical measurements of porcine lumbar vertebrae. *Clin. Biomech. (Bristol., Avon.)* 22:607–613, 2007.

[5]Dickey, J. P., M. R. Pierrynowski, D. A. Bednar, and S. X. Yang. Relationship between pain and vertebral motion in chronic low-back pain subjects. *Clin. Biomech. (Bristol., Avon.)* 17:345–352, 2002.
[6]Doyle, W. Operation useful for similarity-invariant pattern recognition. *J. ACM*. 9:259–267, 1962.
[7]Fujiwara, A., K. Tamai, H. S. An, T. Kurihashi, T. H. Lim, H. Yoshida, and K. Saotome. The relationship between disc degeneration, facet joint osteoarthritis, and stability of the degenerative lumbar spine. *J. Spinal Disord.* 13:444–450, 2000.
[8]Gill, S., P. Abolmaesumi, G. Fichtinger, J. Boisvert, D. Pichora, D. Borshneck, and P. Mousavi. Biomechanically constrained groupwise ultrasound to CT registration of the lumbar spine. *Med. Image Anal.* 16:662–674, 2012.
[9]Grood, E. S., and W. J. Suntay. A joint coordinate system for the clinical description of three-dimensional motions: application to the knee. *J Biomech. Eng.* 105:136–144, 1983.
[10]Haberland, N., K. Ebmeier, J. P. Grunewald, R. Hliscs, and R. L. Kalff. Incorporation of intraoperative computerized tomography in a newly developed spinal navigation technique. *Comput. Aided Surg.* 5:18–27, 2000.
[11]Haque, M. A., W. Anderst, S. Tashman, and G. E. Marai. Hierarchical model-based tracking of cervical vertebrae from dynamic biplane radiographs. *Med. Eng. Phys.* 35:994–1004, 2013.
[12]Haughton, V. M., B. Rogers, M. E. Meyerand, and D. K. Resnick. Measuring the axial rotation of lumbar vertebrae in vivo with MR imaging. *Am. J. Neuroradiol.* 23:1110–1116, 2002.
[13]Hayes, M. A., T. C. Howard, C. R. Gruel, and J. A. Kopta. Roentgenographic evaluation of lumbar spine flexion-extension in asymptomatic individuals. *Spine (Phila Pa 1976)* 14:327–331, 1989.
[14]ISO 5725-2:1994. Accuracy (trueness and precision) of measurement methods and results. Part 2: Basic method for the determination of repeatability and reproducibility of a standard measurement method. 1994.
[15]ISO 5725-4:1994. Accuracy (trueness and precision) of measurement methods and results. Part 4: Basic methods for the determination of the trueness of a standard measurement method. 1994.
[16]Koo, T. K., J. Y. Guo, C. Ippolito, and J. C. Bedle. Assessment of scoliotic deformity using spinous processes: comparison of different analysis methods of an ultrasonographic system. *J. Manip. Physiol. Ther.* 37:667–677, 2014.
[17]Landini, G. Auto threshold. http://fiji.sc/Auto_Threshold. 2015.
[18]McDonald, C. P., C. C. Bachison, V. Chang, S. W. Bartol, and M. J. Bey. Three-dimensional dynamic in vivo motion of the cervical spine: assessment of measurement accuracy and preliminary findings. *Spine J.* 10:497–504, 2010.
[19]Muratore, D. M., B. M. Dawant, and R. L. Galloway. Vertebral surface extraction from ultrasound images for technology-guided therapy. *Proc. SPIE* 3661:1499–1510, 1999.
[20]Nelder, J. A., and R. Mead. A simplex method for function minimization. *Comput. J.* 7:308–313, 1965.
[21]Ochia, R. S., N. Inoue, S. M. Renner, E. P. Lorenz, T. H. Lim, G. B. Andersson, and H. S. An. Three-dimensional in vivo measurement of lumbar spine segmental motion. *Spine (Phila Pa 1976)* 31:2073–2078, 2006.
[22]Olsson, D. M., and L. S. Nelson. The Nelder-Mead simplex procedure for function minimization. *Technometrics* 17:45–51, 1975.
[23]Pearcy, M., I. Portek, and J. Shepherd. Three-dimensional x-ray analysis of normal movement in the lumbar spine. *Spine (Phila Pa 1976)* 9:294–297, 1984.
[24]Prewitt, J. M. S., and M. L. Mendelsohn. The analysis of cell images. *Ann. N. Y. Acad. Sci.* 128:1035–1053, 1966.
[25]Rasoulian, A., P. Abolmaesumi, and P. Mousavi. Feature-based multibody rigid registration of CT and ultrasound images of lumbar spine. *Med. Phys.* 39:3154–3166, 2012.
[26]Rasoulian, A., A. Seitel, J. Osborn, S. Sojoudi, S. Nouranian, V. A. Lessoway, R. N. Rohling, and P. Abolmaesumi. Ultrasound-guided spinal injections: a feasibility study of a guidance system. *Int. J. Comput. Assist. Radiol. Surg.* 10:1417–1425, 2015.
[27]Ron, O., L. Joskowicz, C. Milgrom, and A. Simkin. Computer-based periaxial rotation measurement for aligning fractured femur fragments from CT: a feasibility study. *Comput. Aided Surg.* 7:332–341, 2002.
[28]Shao, W., R. Wu, K. V. Ling, C. H. Thng, H. S. Ho, C. W. Cheng, and W. S. Ng. Evaluation on similarity measures of a surface-to-image registration technique for ultrasound images. *Med. Image Comput. Comput. Assist. Interv.* 9:742–749, 2006.
[29]Singer, S., and J. Nelder. Nelder-Mead algorithm. *Scholarpedia J.* 4:2928, 2009.
[30]Tsao, J., C. P. Chiodo, D. S. Williamson, M. G. Wilson, and R. Kikinis. Computer-assisted quantification of periaxial bone rotation from X-ray CT. *J Comput. Assist. Tomogr.* 22:615–620, 1998.
[31]Weber, P. K., J. C. Schlegel, J. Meiche, L. Peter, and U. Harland. A system for ultrasound-based intraoperative navigation in spine-surgery. *IEEE Int. Ultrasound Symp.* 2:1361–1364, 2001.
[32]Wever, D. J., A. G. Veldhuizen, J. P. Klein, P. J. Webb, G. Nijenbanning, J. C. Cool, and J. R. Horn. A biomechanical analysis of the vertebral and rib deformities in structural scoliosis. *Eur. Spine J.* 8:252–260, 1999.
[33]Winter, S., B. Brendel, I. Pechlivanis, K. Schmieder, and C. Igel. Registration of CT and intraoperative 3-D ultrasound images of the spine using evolutionary and gradient-based methods. *IEEE Trans. Evolut. Comput.* 12:284–296, 2008.
[34]Winter, S., I. Pechlivanis, C. Dekomien, C. Igel, and K. Schmieder. Toward registration of 3D ultrasound and CT images of the spine in clinical praxis: design and evaluation of a data acquisition protocol. *Ultrasound Med. Biol.* 35:1773–1782, 2009.
[35]Yan, C. X., B. Goulet, J. Pelletier, S. J. Chen, D. Tampieri, and D. L. Collins. Towards accurate, robust and practical ultrasound-CT registration of vertebrae for image-guided spine surgery. *Int. J. Comput. Assist. Radiol. Surg.* 6:523–537, 2011.
[36]Yan, C. X., B. Goulet, D. Tampieri, and D. L. Collins. Ultrasound-CT registration of vertebrae without reconstruction. *Int. J. Comput. Assist. Radiol. Surg.* 7:901–909, 2012.